

Calculating the Coulomb blockade phase diagram in the strong coupling regime of single-electron transistor: a quantum Monte Carlo study

Pipat Harata, Wipada Hongthong and Prathan Srivilai*

NanoMaterials Physics Research Unit (NMPRU), Department of Physics, Faculty of Science, Mahasarakham University, Khamriang Sub-District, Kantarawichai District, Mahasarakham 44150, Thailand

E-mail: prathan.s@msu.ac.th

January 2024

Abstract. We present a novel approach for calculating the Coulomb Blockade Phase Diagram (CBPD) in the experimentally accessible strong coupling regime of a single-electron transistor (SET). Our method utilizes the Path Integral Monte Carlo (PIMC) technique to accurately compute the Coulomb oscillation of the Differential Capacitance (DC). Furthermore, we investigate the impact of the gate voltage and temperature variations on the DC, thereby gaining insights into the system's behaviour. As a result, we propose a method to calculate the Coulomb Blockade Boundary Line (CBBL) and demonstrate its efficacy by setting the visibility parameter to 10%. The resulting boundary line effectively defines the transition between the Coulomb and non-Coulomb blockade regimes, thereby enabling the construction of a comprehensive CBPD.

Keywords: Coulomb blockade phase diagram, single-electron transistor, Coulomb blockade effect

1. Introduction

Single-electron devices [1, 2] have attracted attention continuously due to their nanoscale size, low power dissipation, and ability to offer novel functionalities. However, realizing the Coulomb blockade effect in nanoscale junction systems necessitates fulfilling two crucial conditions [1, 3]. Firstly, the kinetic energy of the electrons must be considerably lower than the charging energy to suppress thermal fluctuations that could obscure the quantization effect. Secondly, electrons must be confined or localized on the island, necessitating a tunnelling barrier with resistance much more significant than the quantum resistance unit. These conditions are essential to ensure the proper operation and manifestation of the Coulomb blockade effect. The focus of the theoretical study is on the optimization of these two critical Coulomb blockade effect parameters. This

optimization is represented as a CBPD, which features a boundary line separating the Coulomb blockade regime from the Non-Coulomb blockade regime [4]. By referring to the CBPD, researchers can determine the extent of the Coulomb blockade effect in investigations involving single-electron devices.

A low-conductance SET can be defined as its dimensionless parallel conductance, $g < 1$, where $g = (G_S + G_D)/G_K$, with G_S and G_D are the high-temperature conductance of tunneling junctions connected with source and drain electrodes, as depicted in Fig. 1(a), and the quantum conductance $G_K = e^2/h$. Applying Green's non-equilibrium function approach [5, 6, 7], the CBPD for a low-conductance SET was calculated [4] and referred to as a weak coupling regime [8, 9, 10]. Utilizing the proposed method, one can determine the optimum temperature to operate a low-conductance SET for various applications, such as single-electron memory [11, 12, 13] and quantum dots [14], which trap and manipulate individual electrons, allowing researchers to explore quantum phenomena. On the other hand, a high-conductance SET, i.e., $g \geq 1$, is well-known for its sensitivity to single-electron charges, which qualifies it for terahertz electronics [15, 16], ultra-sensitive sensor applications [17, 18], and qubits in quantum computing [19]. The CBPD, however, cannot be determined using Green's non-equilibrium function method since it exceeds the limits of perturbation theory [8, 9, 10]. As a result, there needs to be more theoretical study in the field of nanoscience. Consequently, this paper proposes a calculation of the CBPD for a high-conductance SET, known as a strong coupling regime [20, 21, 22, 23, 24].

This paper presents an approach for calculating the CBPD within the experimentally accessible strong coupling regime [25]. Our method aims to characterize the charge fluctuation within the SET. Initially, we calculate the Coulomb oscillation of the DC [26, 27] by the PIMC technique [28, 29, 30], which provides valuable insights into the system's behavior. Subsequently, we calculate the visibility parameter [26, 27, 31], quantifying the disparity between the minimum and maximum magnitudes of the DC. By leveraging the visibility parameter, we can calculate the boundary line separating the Coulomb blockade regime from the Non-Coulomb blockade regime. This proposed methodology allows for a more thorough investigation of the behavior of the SET system and provides an enhanced understanding of the system's behavior without coupling limitations.

The sections of this paper are structured as follows: Section 2 provides an introduction to the Hamiltonian governing the SET system, along with basic notations pertinent to the path integral representation employed for the DC calculations. Section 3 presents the results of the DC simulation by utilizing the PIMC technique. Additionally, this section explores the impact of the temperature variations and tunnelling conductance on the measured DC. Subsequently, Section 4 introduces the calculation for the visibility parameter and determines the precise boundary line and the CBPD. Lastly, in Section 5, we offer concluding remarks on the findings of this study and discuss potential avenues for future research in this domain.

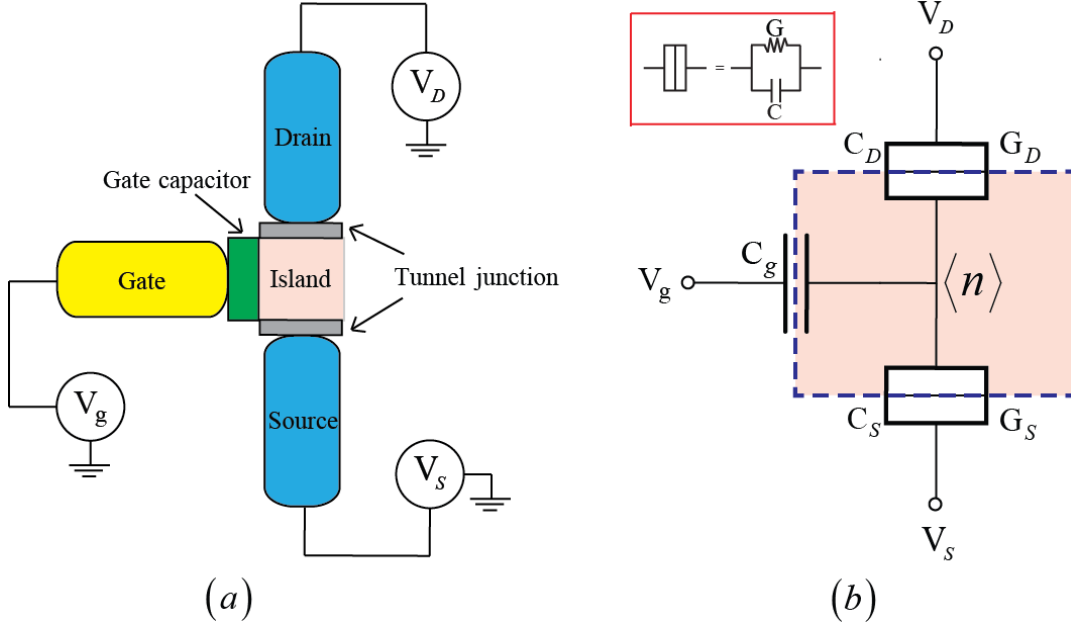


Figure 1. According to the schematic structure (a), the SET system comprises two tunnel junctions and a capacitive junction. The voltage differential, $V_D - V_S$, defines the bias configuration, while the gate voltage V_g is directly coupled to the island via the gate capacitance C_g . The central portion of the SET, denoted by the blue dashed line, encompasses the region where excess electrons n are contained (b)

2. Model Hamiltonian and Differential Capacitance Calculation

2.1. Model Hamiltonian

Consider the arrangement in Fig. 1(a), where the voltage gate controls the electrostatic potential on a metallic island connecting two tunnel junctions, and Fig. 1(b) shows its equivalent circuit. In this two primary dimensionless parameters can govern the transport properties of the SET [25]. Firstly, the dimensionless inverse temperature βE_C is the ratio of the charging energy to the electron's kinetic energy, where the charging energy $E_C = e^2/2C_\Sigma$ with the total capacitance $C_\Sigma = C_S + C_D + C_g$ and $\beta = 1/k_B T$. Secondly, the dimensionless parallel conductance, (g), represents the strength of tunneling phenomena, accessible by measuring the high-temperature conductance of two tunneling junctions [25].

The quantum transport properties of the SET can be effectively described by considering the electrostatic charge and electron tunnelling between the leads and the island. Furthermore, in the metallic island system, the impact of energy quantization can be disregarded due to the negligible spacing between the island states on the metallic island compared to the charging energy. Consequently, it is possible to construct a microscopic model of the SET using the Hamiltonian represented by [1]

$$H = H_B + H_T + H_C, \quad (1)$$

where the conduction electrons of the leads and the island are expressed by

$$H_B = \sum_{Jk\sigma} \epsilon_{Jk\sigma} c_{Jk\sigma}^\dagger c_{Jk\sigma} + \sum_{k\sigma} \epsilon_{k\sigma} d_{k\sigma}^\dagger d_{k\sigma}, \quad (2)$$

respectively. Here $\epsilon_{Jk\sigma}$ is the energy of an electron with a longitudinal wave vector k in channel σ of lead J , where $J \in \{S, D\}$. Likewise, $\epsilon_{k\sigma}$ is the energy of an electron on the island. $c_{Jk\sigma}$ and $d_{k\sigma}$ are the corresponding electron annihilation operator of lead J and the island with longitudinal wave vector k in channel σ .

The tunnelling of the electrons across the two tunnel junctions is described by

$$H_T = \sum_{kq\sigma} \left[d_{k\sigma}^\dagger t_{Skq\sigma} e^{-i\varphi} c_{Sq\sigma} + c_{Dk\sigma}^\dagger t_{Dkq\sigma} e^{i\varphi} d_{q\sigma} + \text{H.c.} \right], \quad (3)$$

where $t_{Skq\sigma}$ is the amplitude for an electron in state $|q\sigma\rangle$ on the source lead tunnel onto the island with the final state $|k\sigma\rangle$. Likewise, $t_{Dkq\sigma}$ denotes the electron tunnelling amplitude of the tunnel junction between the island and the drain lead. The charge shift operator $e^{-i\varphi}$ adds one charge to the island, corresponding with the phase operator φ conjugating to the number operator n of the excess charge on the island. Here we defined $\varphi_S = \varphi_D = 0$ and $\hbar = 1$ through this letter.

The charging energy, denoted as $H_C = E_C(n - n_g)^2$, represents the effect of the (excess) electron numbers n on the island, and $n_g = C_g V_g / e$ is the continuous charge induced by the gate voltage. By starting from the Hamiltonian presented in Eq.(1), the evaluation of the grand partition function, $Z = \text{tr} \{ e^{-\beta(H - \mu \hat{N})} \}$, for the SET can be accomplished by applying the imaginary-time path integral representation [29] and utilizing the large channel approximation [8, 32, 33]. In this context, μ and \hat{N} stand for the system's chemical potential and the particle number operator, respectively. However, we skip the detailed calculation procedure as it has been thoroughly addressed in the provided reference [34]. Therefore, all possible paths are expressed in imaginary time, and we can perform the quantum Monte Carlo method [28, 29, 30] to analyse the quantum statistical characteristics of the SET.

2.2. Differential Capacitance Calculation

The average excess tunnelling charge can effectively characterize the quantum transport properties and Coulomb blockade effect of the SET [9, 21, 24, 35, 36, 37]. In particular, the variation in the average tunnelling charge on the island concerning the gate voltage can be represented by $C_{\text{diff}} = \partial \langle Q_t \rangle / \partial V_g$ [26, 27]. Here the average tunnelling charge is $\langle Q_t \rangle = -e \langle n \rangle$, and $\langle n \rangle$ represents the island's average (excess) electron number. Consequently, the average electron number can be calculated by $\langle n \rangle = n_g + (2\beta E_C)^{-1} (\partial \ln Z / \partial n_g)$ [38]. As a result, the DC of the SET can be expressed in terms of the winding number and represented by

$$\frac{C_{\text{diff}}}{C_g} = \frac{d \langle n \rangle}{dn_g} = 1 - \frac{2\pi^2}{\beta E_C} \left(\langle k^2 \rangle - \langle k \rangle^2 \right), \quad (4)$$

where the winding number expectation value can be represented in terms of the path integral representation as

$$\langle X \rangle = \frac{\sum_{k=-\infty}^{\infty} \int_{\xi(0)=0}^{\xi(\beta E_C)=0} D\xi X e^{-S[\xi,k]}}{\sum_{k=-\infty}^{\infty} \int_{\xi(0)=0}^{\xi(\beta E_C)=0} D\xi e^{-S[\xi,k]}}. \quad (5)$$

Here all energies are measured in units of the charging energy E_C to make the PIMC simulation more convenient. The partition function, typically expressed as a path integral over the phase variable φ , has been obtained through the transformation $\varphi(\tau) = \xi(\tau) + \nu_k \tau$ with $\nu_k = (2\pi k / \beta E_C)$, and the utilization of the boundary condition of the paths $\xi(0) = \xi(\beta E_C)$. As a result, the Euclidean action of the SET, denoted as $S[\xi, k] = S_C[\xi, k] + S_T[\xi, k]$, can be represented in terms of the Coulomb action,

$$S_C[\xi, k] = \int_0^{\beta E_C} d\tau \left(\frac{\dot{\xi}^2}{4} \right) + \frac{4\pi^2 k^2}{\beta E_C} + 2\pi i k n_g, \quad (6)$$

where $\dot{\xi} = (d\xi/d\tau)$ and the tunnelling action,

$$S_T[\xi, k] = -g \int_0^{\beta E_C} d\tau \int_0^{\beta E_C} d\tau' \alpha(\tau - \tau') \cos(\xi(\tau) - \xi(\tau') + \nu_k(\tau - \tau')), \quad (7)$$

where the tunnelling kernel reads

$$\alpha(\tau) = \frac{1}{4(\beta E_C)^2 \sin^2\left(\frac{\pi}{\beta E_C} \tau\right)}. \quad (8)$$

The exact solution for the expectation value of the winding number, as described in Eq.(5), cannot be obtained through analytical calculations due to its non-Gaussian integral nature. However, the winding number's expectation value and the DC of the SET can be evaluated using the PIMC technique.

2.3. PIMC simulation of the winding number expectation value

In this subsection, we summarized the essential details of the PIMC simulation for the SET following the main idea in Ref. [34]. The PIMC technique was employed to simulate the DC results of the SET across the entire range of the dimensionless gate voltage, $n_g \in \{0, 1\}$, the inverse temperature, $\beta E_C \in \{1, 21\}$, and specifically at high dimensionless conductance, $g \in \{1, 15\}$, where the perturbation theory fails. In order to utilize the Metropolis algorithm [39, 40], a positive definite action is required. Consequently, we must include the imaginary part of the Coulomb action in

the observable to be measured, i.e., $\exp\{-2\pi i n_g k\}$, and use the fact that the expectation value of the odd function is zero. The expectation values in Eq.(4) can be rewritten as

$$\langle k \rangle = \frac{\langle k \sin(2\pi n_g k) \rangle_0}{\langle \cos(2\pi n_g k) \rangle_0}, \quad (9)$$

and

$$\langle k^2 \rangle = \frac{\langle k^2 \cos(2\pi n_g k) \rangle_0}{\langle \cos(2\pi n_g k) \rangle_0}, \quad (10)$$

where $\langle X \rangle_0$ denotes the expectation value with the positive action

$$S_0[\xi, k] = \int_0^{\beta E_C} d\tau \left(\frac{\dot{\xi}^2}{4} \right) + \frac{4\pi^2 k^2}{\beta E_C} - S_T[\xi, k]. \quad (11)$$

The discrete formula of Eq.(9) used in the PIMC simulation is

$$\langle k \rangle = \frac{\sum_{k_j \in \{k, \xi\}} k_j \sin(2\pi k_j n_g)}{\sum_{k_j \in \{k, \xi\}} \cos(2\pi k_j n_g)}, \quad (12)$$

where the sum $\sum_{k_i \in \{k, \xi\}}$ stands for the accumulation of k_j over the configurations ξ and k sampled by the Metropolis algorithm for the positive action in Eq.(11). The expectation value in Eq.(10) can proceed similarly. The results for the winding number expectation values over the whole range of gate voltages can be obtained from a single Monte Carlo simulation since the positive action is independent of n_g . In addition, the DC results were obtained through extensive Monte Carlo simulations, employing multiple measurements to ensure the statistical error remained below a certain threshold, i.e., 1%, across the entire parameter ranges. Consequently, the error bars displayed in the Monte Carlo data indicate that the magnitude of one standard deviation is smaller than the symbol size depicted in all the following figures.

3. Results and Discussions

The DC results of the SET were simulated using the PIMC technique, focusing on the dimensionless gate voltage range denoted as $n_g \in \{0, 1\}$. Fig. 2 presents the results for two specific conditions: the absence of any bias between the source and drain electrodes and the strong tunnelling regime characterized by $g \geq 1$. In Fig. 2, particular attention is given to the red dotted line, revealing an interesting observation, in which, when $\beta E_C = 1$, the ratio of the DC to the gate capacitance remains constant at unity, independent of the dimensionless gate voltage. This finding implies that the Coulomb blockade effect ceases to exist since the charging energy becomes approximately equal to the kinetic energy of the electrons. Conversely, as the temperature decreases with a corresponding increase in βE_C , the DC depends on the dimensionless gate voltage. Notably, the magnitudes of the DC peaks reach their maximum values when $n_g = 0.5$ and their minimum values when $n_g = 0.0$, as illustrated in Fig 2. Consequently, it becomes

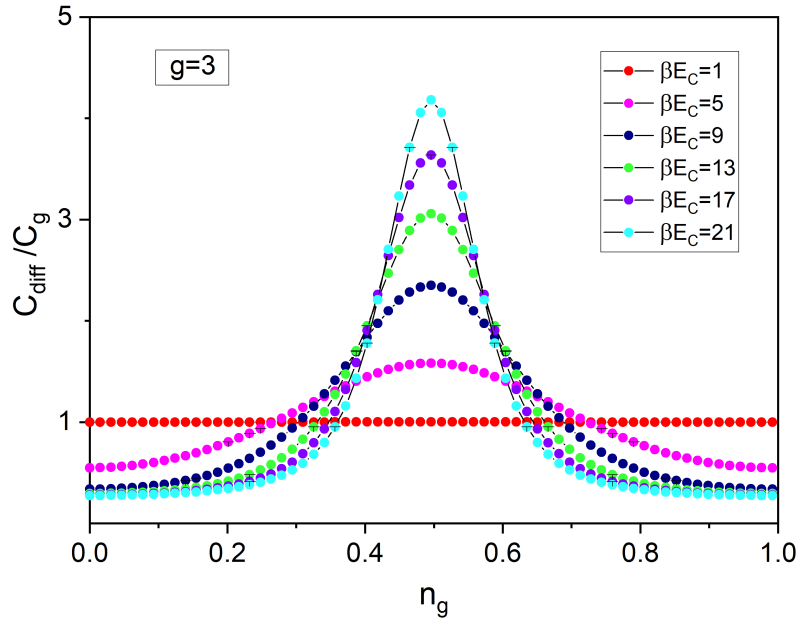


Figure 2. DC of SET exhibits Coulomb oscillations as a function of the dimensionless gate voltage n_g , where the dimensionless conductance is fixed at $g = 3$, while the inverse temperature varies.

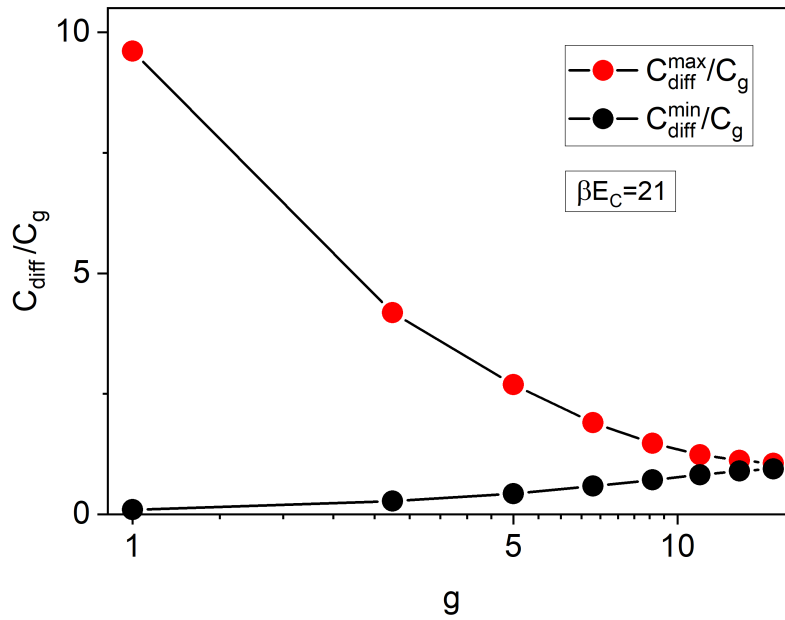


Figure 3. SET's normalized maximum and minimum DC obtained from PIMC simulations, plotted against the inverse temperature ($\beta E_C = 21$) and normalized to the gate capacitance.

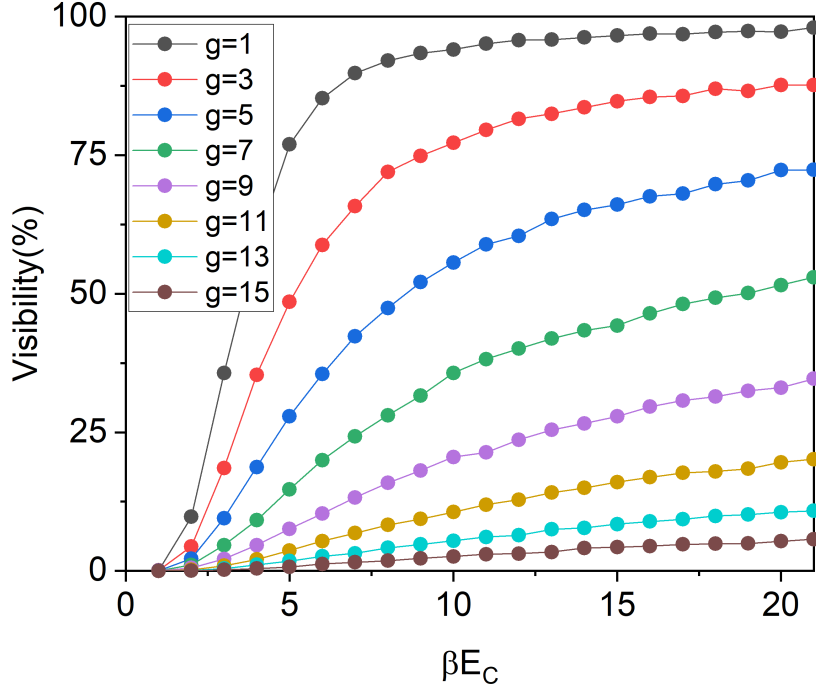


Figure 4. Visibility of SET varies as a function of the inverse temperature for different dimensionless conductance values.

evident from the presence of these peaks in the DC that the Coulomb blockade effect is indeed occurring, provided that the condition $\beta E_C \gg 1$ is satisfied. As described above, the Coulomb oscillation peaks provide clear evidence of the occurrence of the Coulomb blockade effect. The electron localization on the island can be governed by the optimization between parameters g and βE_C , leading to the observed oscillatory behavior in the DC.

Due to the Coulomb blocked effect in the SET being reflected by the Coulomb oscillation in the DC, we can define the minimal and maximal DC at $n_g = 0.0$ and $n_g = 0.5$, denoted by $C_{\text{diff}}^{\text{min}}$ and $C_{\text{diff}}^{\text{max}}$, respectively. By fixed temperature, while the dimensionless conductance varies, the Coulomb oscillation of the DC occurs, reflected as the difference between $C_{\text{diff}}^{\text{min}}$ and $C_{\text{diff}}^{\text{max}}$, as shown in Fig.3. When g increases significantly, the $C_{\text{diff}}^{\text{min}}$ merges with $C_{\text{diff}}^{\text{max}}$, and the Coulomb blockade effect vanishes. As a result, it is indicated that the difference in the magnitudes of $C_{\text{diff}}^{\text{min}}$ and $C_{\text{diff}}^{\text{max}}$ can identify the Coulomb Blockade and Non-Coulomb Blockade regimes. Furthermore, the magnitude of $C_{\text{diff}}^{\text{min}}$ is directly associated with the effective charging energy defined as $E_C^*/E_C = 1 - C_{\text{diff}}^{\text{min}}$. The effective charging energy is widely recognized as a measure of the strength of the Coulomb blockade effect and this has been extensively investigated in the literature [23, 41, 42].

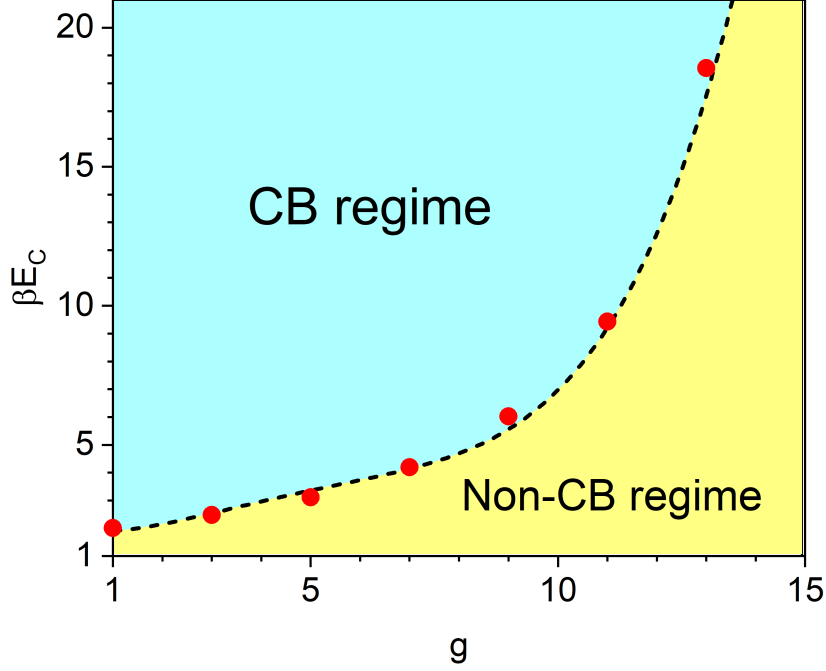


Figure 5. CBPD of SET was calculated with the visibility of 10%, illustrating the boundary line that demarcates the Coulomb and Non-Coulomb blockade regimes. The red circle data points correspond to the results of fitting the PIMC data.

Visibility

More practically, to propose a calculation for a CBBL, the visibility of the SET was defined as

$$\mathbf{V} = \frac{C_{\text{diff}}^{\text{max}} - C_{\text{diff}}^{\text{min}}}{C_{\text{diff}}^{\text{max}} + C_{\text{diff}}^{\text{min}}}. \quad (13)$$

The inverse temperature's effect on the SET's visibility is illustrated in Fig. 4. Consequently, as βE_C increases, the visibility also increases and stabilizes at a constant value determined by the g parameter. Therefore, a CBBL is established through the utilization of Monte Carlo data fitting for the individual parameter g , employing a polynomial function, $\mathbf{V} = C_0 + C_1(\beta E_C) + C_2(\beta E_C)^2$, characterized by constants C_0, C_1 , and C_2 . By assigning a desired visibility value \mathbf{V} , the polynomial equation can be solved to determine the corresponding βE_C value. Consequently, constructing the CBBL involves utilizing a set of ordered pairs $(g, \beta E_C)$.

As a demonstration, Fig. 5 illustrates the CBBL within the phase diagram, providing insights into the SET behaviour. The visibility is set explicitly to $\mathbf{V} = 10\%$, corresponding to $C_{\text{diff}}^{\text{min}}/C_{\text{diff}}^{\text{max}} \sim 0.82$. Mathematically, the CBBL can be described by the polynomial equation as

$$\beta E_C = 2.6465 - 0.9896g + 0.45g^2 - 0.0603g^3 + 0.003g^4. \quad (14)$$

When the condition $\beta E_C > 2.6465 - 0.9896g + 0.45g^2 - 0.0603g^3 + 0.003g^4$ is satisfied, the SET operates within the Coulomb blockade region, denoted by the sky blue area. Conversely, if $\beta E_C < 2.6465 - 0.9896g + 0.45g^2 - 0.0603g^3 + 0.003g^4$, the SET operates outside the Coulomb blockade regime, represented by the yellow region.

Furthermore, the CBBL represented by Eq.(14) can be verified with the SET experiments, known for their parallel dimensionless conductance and temperature operation in terms of βE_C . For example, the experiment of the SET with the dimensionless conductance of $g = 4.75$ was reported as the Coulomb oscillations of conductance [25, 34]. It is easy to predict from Eq.(14) that the Coulomb blockade effect occurs by operating with $\beta E_C > 3.16$. The finding agrees with the Coulomb oscillation experiment shown in Fig. 6.12 of Ref. [34], wherein the Coulomb oscillation peak appears evidently with $\beta E_C > 3.0$. Let us next focus on the first experiment demonstrating a SET operating at room temperature [43]. The aluminum SET fabricated by standard e-beam lithography consists of $g = 0.002$ and was operated at $300 K$. From Eq.(14), one obtains that the condition of the Coulomb blockade occurring is $\beta E_C > 2.644$, corresponding with $504.28 K$, where $E_C = 115 meV$. The result confirms that the SET can exhibit the Coulomb blockade effect at room temperature.

In addition, one can use Eq.(14) to analyze SET experiments. For example, B. Dutta et al. [44] reported the measurements of heat and charge transport through the symmetric SETs called samples A and B, with the parallel dimensionless conductance, $g = 0.629$ (low-conductance SET) and $g = 1.98$ (high-conductance SET), respectively. Eq.(14) shows that the samples A and B are in Coulomb blockade regions for operating with $\beta E_C > 2.187$ and $\beta E_C > 2.029$, respectively. However, they operated the SETs with $\beta E_C > 21.87$ and $\beta E_C > 20.19$, corresponding with $132 mK$ and $152 mK$, where $E_C = 155 \mu eV$ and $E_C = 100 \mu eV$, respectively. That means they operated at about ten times the boundary temperature for their investigations. As described above, the CBBL, determined by the essential parameters g and βE_C , holds significant relevance for both experimental fabrications and theoretical investigations of SETs.

4. Conclusions

In this paper, we have proposed a method to calculate the CBPD of a SET by utilizing the DC Monte Carlo data. Using the PIMC technique, we have demonstrated that the parallel dimensionless conductance and temperature influence the SET's DC expressed in terms of the expected values of the winding number. Furthermore, our study established the range of minimum and maximum DC, providing a means to quantify the strength of the Coulomb blockade effect through the visibility parameter. For example, the CBBL was calculated with a visibility parameter of $\mathbf{V} = 10\%$. The resulting boundary line effectively delineates the transition between the Coulomb and non-Coulomb blockade regimes, allowing for the establishment of a comprehensive CBPD. In addition, SET experiments were introduced to verify the CBPD. We found that the equation of the CBBL can predict the Coulomb blockade effect occurring in

both the low and high-conductance SET. Further, the method presented in this study hold the potential to serve as a standard framework for investigating SET and quantum island systems with increasingly complex topologies.

Acknowledgments

This research project was financially supported by Mahasarakham University for the main funding and the NanoMaterials Physics Research Unit (NMPRU). We especially thank K. Limtragool for valuable discussions.

References

- [1] Grabert H and Devoret M H (eds) 1992 (*NATO ASI series B: Physics* vol 294) (New York: Plenum Press)
- [2] Likharev K 1999 *Proceedings of the IEEE* **87** 606–632
- [3] Devoret M, Esteve D and Urbina C 1992 *Nature* **360**(6404) 547–553
- [4] Wang M, lai Wu R, Yu Y, qing Huang W and Ma Z 2014 *Physica B: Condensed Matter* **454** 82–85 ISSN 0921-4526
- [5] Damle P S, Ghosh A W and Datta S 2001 *Phys. Rev. B* **64**(20) 201403
- [6] Taylor J, Guo H and Wang J 2001 *Phys. Rev. B* **63**(24) 245407
- [7] Louis C N and Iyakutti K 2003 *Phys. Rev. B* **67**(9) 094509
- [8] Grabert H 1994 *Phys. Rev. B* **50**(23) 17364–17377
- [9] König J, Schoeller H and Schön G 1997 *Phys. Rev. Lett.* **78**(23) 4482–4485
- [10] König J and Schoeller H 1998 *Phys. Rev. Lett.* **81**(16) 3511–3514
- [11] Touati A, Chatbouri S and Adel K 2013 *ISRN Nanotechnology* 587436
- [12] Ibukuro K, Husain M K, Li Z, Hillier J, Liu F, Tomita I, Tsuchiya Y, Rutt H and Saito S 2019 *Frontiers in Physics* **7** ISSN 2296-424X
- [13] Nakazato K, Blaikie R J and Ahmed H 1994 *Journal of Applied Physics* **75** 5123–5134 ISSN 0021-8979
- [14] Choi B H, Hwang S W, Kim I G, Shin H C, Kim Y and Kim E K 1998 *Applied Physics Letters* **73** 3129–3131 ISSN 0003-6951
- [15] Asgari M, Coquillat D, Menichetti G, Zannier V, Diakonova N, Knap W, Sorba L, Viti L and Vitiello M S 2021 *Nano Letters* **21** 8587–8594
- [16] Park K S, Kim S J, Paik I B, Lee W H, Kang J S, Cho Y B, Lee S D, Lee C K, Kim J H and Choi J B 2004 *Semiconductor Science and Technology* **19** L39
- [17] Nakajima A 2016 *Applied Sciences* **6** ISSN 2076-3417
- [18] Cleland A N, Esteve D, Urbina C and Devoret M H 1993 *Journal of Low Temperature Physics* **93** 767–772 ISSN 1573-735
- [19] Aassime A, Johansson G, Wendin G, Schoelkopf R J and Delsing P 2001 *Phys. Rev. Lett.* **86**(15) 3376–3379
- [20] Schoeller H and Schön G 1994 *Phys. Rev. B* **50**(24) 18436–18452
- [21] Joyez P, Bouchiat V, Esteve D, Urbina C and Devoret M H 1997 *Phys. Rev. Lett.* **79**(7) 1349–1352
- [22] Wang X, Egger R and Grabert H 1997 *Europhys. Lett.* **38** 545–550
- [23] Herrero C P, Schön G and Zaikin A D 1999 *Phys. Rev. B* **59**(8) 5728–5737
- [24] Göppert G, Hüpper B and Grabert H 2000 *Phys. Rev. B* **62**(15) 9955–9958
- [25] Wallisser C, Limbach B, vom Stein P, Schäfer R, Theis C, Göppert G and Grabert H 2002 *Phys. Rev. B* **66**(12) 125314
- [26] Jezouin S, Iftikhar Z, Anthore A, Parmentier F D, Gennser U, Cavanna A, Ouerghi A, Levkivskiy I P, Idrisov E, Sukhorukov E V, Glazman L I and Pierre F 2016 *Nature* **536**(7614) 58–62

- [27] Idrisov E G, Levkivskiy I P and Sukhorukov E V 2017 *Phys. Rev. B* **96**(15) 155408
- [28] Ceperley D M 1995 *Rev. Mod. Phys.* **67**(2) 279–355
- [29] Negele J W and Orland H 1987 *Quantum Many-Particle Systems (Frontier in Physics)* (AddisonWesley)
- [30] Troyer M and Wiese U J 2005 *Phys. Rev. Lett.* **94**(17) 170201
- [31] Limmer D T, Merlet C, Salanne M, Chandler D, Madden P A, van Roij R and Rotenberg B 2013 *Phys. Rev. Lett.* **111**(10) 106102
- [32] Ambegaokar V, Eckern U and Schön G 1982 *Phys. Rev. Lett.* **48**(25) 1745–1748
- [33] Göppert G, Grabert H and Beck C 1999 *Europhys. Lett.* **45** 249–255
- [34] Theis C 2004 *Conductance of Single Electron Devices from Imaginary -Time Path Integrals* PhD dissertation Freiburg (Breisgau), University, Dissertation, available as pdf. under <https://freidok.uni-freiburg.de/fedora/objects/freidok:1328/datastreams/FILE1/content>
- [35] König J, Schoeller H and Schön G 1998 *Phys. Rev. B* **58**(12) 7882–7892
- [36] Chouvaev D, Kuzmin L S, Golubev D S and Zaikin A D 1999 *Phys. Rev. B* **59**(16) 10599–10602
- [37] Devoret M H and Schoelkopf R J 2000 *Nature* **406**(6799) 1039–1046
- [38] Göppert G and Grabert H 2001 *Phys. Rev. B* **63**(12) 125307
- [39] Metropolis N, Rosenbluth A W, Rosenbluth M N, Teller A H and Teller E 1953 *The Journal of Chemical Physics* **21** 1087–1092 ISSN 0021-9606
- [40] Grotendorst J 2002 *Quantum Simulations of Complex Many Body Systems: from Theory to Algorithms: Euro Winter School 25 February - 1 March 2002, Rolduc Conference Centre Kerkrade, The Netherlands ; Audio Visual Lecture Notes* NIC series (NIC)
- [41] Werner P and Troyer M 2005 *Journal of Statistical Mechanics: Theory and Experiment* **2005** P01003
- [42] Lukyanov S L and Werner P 2006 *Journal of Statistical Mechanics: Theory and Experiment* **2006** P11002–P11002
- [43] Pashkin Y A, Nakamura Y and Tsai J S 2000 *Applied Physics Letters* **76** 2256–2258 ISSN 0003-6951
- [44] Dutta B, Peltonen J T, Antonenko D S, Meschke M, Skvortsov M A, Kubala B, König J, Winkelmann C B, Courtois H and Pekola J P 2017 *Phys. Rev. Lett.* **119**(7) 077701